CFD Modeling and Simulation in Materials Processing 2016
Edited by: Laurentiu Nastac, Lifeng Zhang, Brian G. Thomas, Miaoyong Zhu, Andreas Ludwig, Adrian S. Sabau, Koulis Pericleous, and Hervé Combeau
TMS (The Minerals, Metals & Materials Society), 2016

VALIDATION OF A MODEL FOR THE COLUMNAR TO EQUIAXED TRANSITION WITH MELT CONVECTION

Mahdi Torabi Rad[1], Christoph Beckermann[1]

[1]Department of Mechanical and Industrial Engineering, The University of Iowa, 2402 SC, Iowa City, IA, 52242, USA

Keywords: Columnar-to-Equiaxed Transition, Melt Convection, Multi-phase/-scale Modeling, Recalescence, OpenFOAM

Abstract

Predicting the columnar-to-equiaxed transition (CET) in the grain structure of metal castings is still an important challenge in the field of solidification. One of the most important open questions is the role played by melt convection. A three-phase Eulerian volume-averaged model of the CET in the presence of melt convection is developed. The model is validated by performing simulations of a recent benchmark solidification experiment involving a Sn - 3 wt. pct. Pb alloy. The predicted cooling curves are found to be in a good agreement with the experimental measurements. After some adjustments to the grain nucleation parameters, the measured boundary between columnar and equiaxed grains is also well predicted.

Introduction

The transition from the elongated grains in the outer portions of a casting to more rounded ones in the center is called *columnar-to-equiaxed transition* (CET) [1]. Realistic modeling and simulation of the CET is still very challenging, because it requires one to simultaneously take into account numerous physical phenomenon at several length scales: heat/solute transfer, melt flow, nucleation of equiaxed grains, and growth of columnar and equiaxed grains into an undercooled melt.

In the past decade, there have been numerous modeling efforts to address this challenging problem. Most of these models are based on the pioneering work of Wang and Beckermann [2]. These authors developed a three-phase volume-averaged Eulerian solidification model, which accounts for phenomena such as: equiaxed dendritic growth, melt flow, micro-/macro-segregation, and transport of solid. Wang and Beckermann [3] and Martorano et al. [4] used a similar model to predict the CET in experimental castings. However, these efforts all neglected melt convection. Wu et al. [5] introduced a five-phase volume-averaged model for the CET in the presence of the melt convection. Their main motivation behind adding two additional phases was to more realistically incorporate the (columnar/equiaxed) dendrite morphology into the model. They have used this model to predict the CET in Al-Cu castings [6].

A benchmark solidification experiment, involving solidification of Sn-Pb alloys was performed by Hachani et al. [7, 8]. Carozzani et al. [9] simulated this experiment using a CAFÉ model. However, some discrepancies were observed between the measurements and the simulation results; especially, in the prediction of the recalescence and the boundary between the columnar and equiaxed grains. They attributed this to uncertainties in the nucleation law.

The main objective of the present study is to briefly introduce and, then, validate a three-phase Eulerian model for the CET in the presence of the melt convection. In the following, the equations of the model are shortly outlined for completeness. The model is then used to predict the cooling curves and the CET in the solidification benchmark experiment of Hachani et al. [4, 5].

The Multi-Phase/-Scale Model

The model we introduce here is a modified version of the model developed by Wang and Beckermann (WB) [2]. The model accounts for the CET in the presence of the melt convection by tracking the position of the columnar front. The solid is assumed to be stationary.

Conservation Equations

Energy Equation:

$$\frac{\partial T}{\partial t}+\nabla\cdot\left(g_l\overline{\boldsymbol{v}}_l T\right)=\alpha_0\nabla^2 T+\frac{h_{sl}}{c_0}\frac{\partial g_s}{\partial t} \tag{1}$$

where T is the temperature, g_l is the liquid fraction, $\overline{\boldsymbol{v}}_l$ is the average liquid velocity, α_0, h_{sl}, c_0 and $g_s\left(=1-g_l\right)$ are the thermal diffusivity, latent heat, specific heat and solid fraction, respectively.

Solute conservation equation for the solid:

$$g_s\frac{\partial \overline{C}_s}{\partial t}=\left(k_0\overline{C}_d-\overline{C}_s\right)\frac{\partial g_s}{\partial t} \tag{2}$$

where $\overline{C}_s$ and $\overline{C}_d$ are the average solute concentration in the solid and the inter-dendritic liquid, respectively, and k_0 is the partition coefficient.

Solute conservation equation for the inter-dendritic liquid:

$$\left(1-k_0\right)\overline{C}_d\frac{\partial g_s}{\partial t}=\left(1-g_s\right)\left(\frac{\partial \overline{C}_d}{\partial t}+\overline{\boldsymbol{v}}_l\cdot\nabla\overline{C}_d\right)+\frac{\partial}{\partial t}\left[g_e\left(\overline{C}_e-\overline{C}_d\right)\right]+\nabla\cdot\left[g_e\overline{\boldsymbol{v}}_l\left(\overline{C}_e-\overline{C}_d\right)\right] \tag{3}$$

where g_e is the extra-dendritic liquid fraction, and $\overline{C}_e$ is the average solute concentration in the extra-dendritic liquid.

Solute conservation equation for the extra-dendritic liquid:

$$g_e \frac{\partial \overline{C}_e}{\partial t} + \nabla \cdot \left(g_e \overline{\boldsymbol{v}}_l \overline{C}_e \right) = D_0 \nabla \cdot \left(g_e \nabla \overline{C}_e \right) + \left(\overline{C}_d - \overline{C}_e \right) \frac{\partial g_e}{\partial t} + \overline{C}_d \nabla \cdot \left(g_e \overline{\boldsymbol{v}}_l \right) + \frac{S_{ed} D_0}{l_{ed}} \left(\overline{C}_d - \overline{C}_e \right) \qquad (4)$$

where D_0 is the liquid mass diffusivity, S_{ed} is the interfacial area concentration, and l_{ed} is the diffusion length.

Mixture continuity and momentum conservation equations:

$$\nabla \cdot \left(g_l \overline{\boldsymbol{v}}_l \right) = 0 \qquad (5)$$

$$\frac{\partial}{\partial t} \left(g_l \overline{\boldsymbol{v}}_l \right) + \frac{1}{g_l} \nabla \cdot \left(g_l^2 \overline{\boldsymbol{v}}_l \overline{\boldsymbol{v}}_l \right) = -\frac{1}{\rho_0} g_l \nabla \overline{p} \; + \upsilon_0 \nabla^2 \left(g_l \overline{\boldsymbol{v}}_l \right) + \frac{\tilde{\rho}_l}{\rho_0} g_l \boldsymbol{g} - \frac{\upsilon_0}{K} g_l^2 \overline{\boldsymbol{v}}_l \qquad (6)$$

where ρ_0 is the reference density, $\overline{p}$ is the average pressure, υ_0 is the kinematic viscosity, $\tilde{\rho}_l$ is the liquid density, given by the Boussinesq approximation, i.e. $\tilde{\rho} = 1 - \beta_T \left(T - T_{ref} \right) - \beta_C \left(\overline{C}_e - C_{ref} \right)$, where, β_T and β_C are the thermal and solutal expansion coefficients, and T_{ref} and C_{ref} are the reference temperature and concentration, at which ρ_0 is determined; and K is the permeability of the mush, given by the Blake-Kozeny equation, i.e. $K = \lambda_2^2 g_l^3 \Big/ \left[180 \left(1 - g_l \right)^2 \right]$.

Supplementary Relations

Supplementary relations of the model are: 1) the liquidus line of the phase diagram [4], 2) an equation for the grain fraction [3], 3) the LGK growth model for the dendrite tip velocity [4], 4) a morphological equation for the interfacial area concentration [4], 5) an equation for the diffusion length [4], 6) the instantaneous nucleation law for the grain nucleation [4], and 7) an equation for tracking the columnar front. Due to space limitations, these models are not provided here.

Simulation of the Benchmark Solidification Experiment

Outline of the Experimental Conditions

Figure 1 shows the sketch of the experimental setup in Hachani et al. [7, 8]. The reader should consult these papers for more details on the experimental procedure. The corresponding material properties, boundary and initial conditions used in the present study are adopted from Carozzani et al. [9].

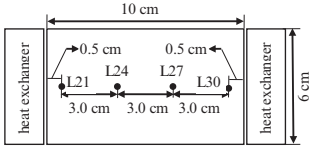

Figure 1. Sketch of the solidification benchmark experiment, performed by Hachani et al. [7, 8], along with the label and the location of the four thermocouples used in the present study to validate the present multi-phase/-scale model.

Numerical Simulations

We developed a parallel-computing in-house code on the OpenFOAM platform to solve the governing equations. In this section, we will only briefly introduce the interface-tracking algorithm that is required to solve these equations. The interested reader should contact the corresponding author for more numerical details.

Solving the equations of the model requires one to track the movement of the columnar front [4]. Here, we assume that these movements are perpendicular to the local isotherms; and then, the columnar front is tracked using the volume-of-fluid method (VOF) [10 and references therein].

Results and Discussion

Prediction of the Measured Cooling Curves

Figure 2 compares the measured cooling curves (empty squares) with the cooling curves predicted by the model (the blue lines) at four different locations shown if Figure 1. The overall agreement between the simulated and the measured temperatures is good.

The recalescence, recorded at position L21 in the experiment, is also well predicted by the model. This is shown in Figure 3, which is a close-up of the cooling curve in Figure 2 (a) around $t = 3500$ s. The grain/solid fractions (to be read from the right vertical axis) are shown by red lines. The liquidus temperature ($T_{liq} = 501.28$ K) and the nucleation temperature ($T_{nuc} = 498.3$ K) are shown by dotted lines. The liquidus temperature is taken from Carozzani et al. [9]; and the nucleation temperature is taken to be the minimum in the measured cooling curve before recalescence. The equiaxed grain density is $n = 10^6$ m^{-3}. We have chosen this value because it gives the best recalescence agreement with the experiment. Before the start of the solidification at this point, ($t < 3490$ s) there is an excellent agreement between the simulated and the measured temperatures. However, the predicted maximum recalescence temperature (=499.2 K) is 0.4 K lower than the measured one (=499.6 K). The reason for this under-prediction is not fully clear at this stage, but it might be because of the uncertainties in the equations used for the diffusion length, or the specific are concentrations. The authors are performing further investigations to clarify this. The outcome of these ongoing investigations will be used to improve the model for a better prediction of the recalescence temperature.

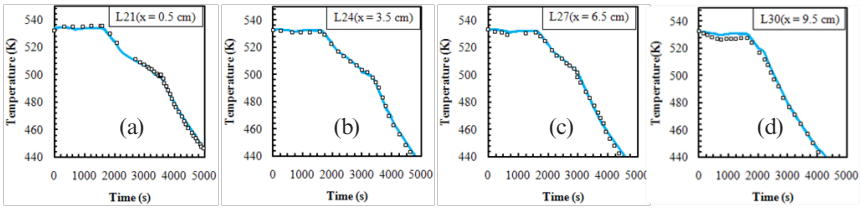

Figure 2. Comparison between the measured [7](symbols) and the simulated(blue lines) cooling curves for four different locations, shown in Figure 1: (a) x = 0.5 cm, (b) x = 3.5 cm, (c) x = 6.5 cm, (d) x = 9.5 cm. The distances are measured from the left boundary.

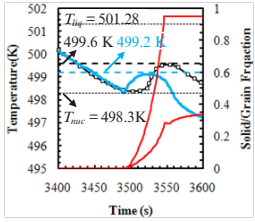

Figure 3. Close-up of the cooling curve shown in Figure 2(a), comparing the measured recalescence [7] (symbols) and the simulated recalescence (blue line), along with the solid/grain fractions (red lines, to be read from the right vertical axis). The dotted lines show the liquidus (501.3 K) and the nucleation (498.3 K) temperatures. The dashed lines indicate the measured (499.6 K) and simulated (499.2 K) recalescence temperatures.

Comparison with Model that Neglects Dendrite Tip Undercooling

Figure (4) compares the results of the model introduced in the present study (top row) with the results of a model that neglects dendrite tip undercooling and assumes Scheil type solidification. (bottom row). The reader is referred to Guo and Beckermann [11] for the equations of the latter model; for simplicity, this model is referred to in the following as the Scheil model. The red line in the top row is the columnar front. In the bottom row, this line is the mushy zone edge (i.e. isoline $g_s = 0.001$). The columns show the results at three different solidification stages. Next, we will compare the top and bottom rows of the figure to investigate the effect of tip undercooling.

At the early solidification stage (i.e. $t = 2400$ s), the predictions of the two models are shown in the first column of figure (4). Again, the contour plot at the top is the model presented here (which accounts for tip undercooling), and the contour plot at the bottom is the Scheil model (which does not account for the tip undercooling). The two contour plots are very similar. In both, the lead-rich heavier fluid moves downward along the solidification front, and generates a clock-wise rotating convection cell. In addition, the columnar front at the top is almost at the same position as the mushy zone edge at the bottom. These similarities indicate that the tip undercooling does not play a significant role at the early solidification stage.

At an intermediate solidification stage (i.e. $t = 3500$ s), the predictions of the two models are shown in the second column of figure (4). Close to the left wall, the two models have very different predictions: while the model introduced here predicts a solid-free zone over the left third of the cavity, the Scheil model predicts mush to present everywhere. The solid fraction patterns predicted by the two models over the right portion of the cavity are also somewhat different, with the Scheil model showing more pronounced channel segregates. These differences between the two models

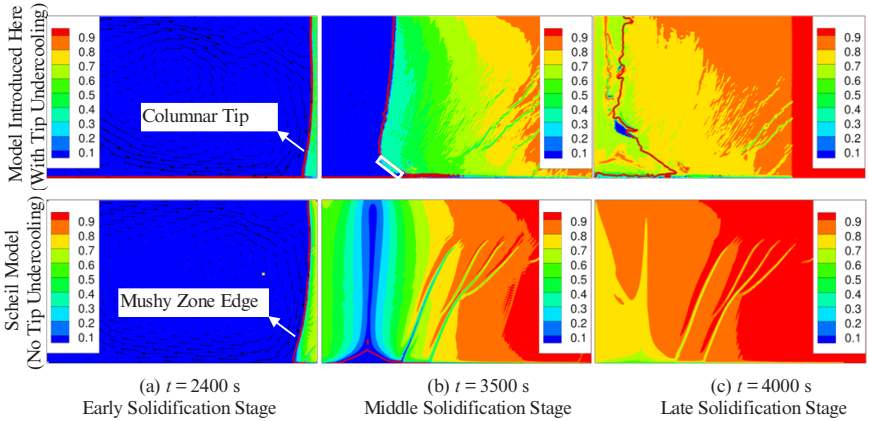

(a) $t = 2400$ s
Early Solidification Stage

(b) $t = 3500$ s
Middle Solidification Stage

(c) $t = 4000$ s
Late Solidification Stage

Figure 4(a-c). Comparison of the predictions of the model introduced in the present study (top row) with the Scheil solidification model (bottom row). Only the former one accounts for tip undercooling. The columns are, from the left: early, middle, and late solidification stages. The color is the solid fraction; and the black arrows are the flow velocity vectors. The red line in the top row is the columnar tip, and in the bottom row, it is the edge of the mushy zone (i.e. isoline $g_s = 0.001$). The inclined white box in the top middle contour shows the appearance of the first equiaxed grains in front of the columnar tip.

indicate that at the intermediate solidification stage, dendrite tip undercooling does play an import role.

At the late solidification stage (i.e. $t = 4000$ s), the predictions of the models are shown in the third column of figure (4). Close to the left wall, the Scheil model predicts slightly higher solid fractions, which can be attributed to this model predicting higher solid fractions at this location at earlier times. Other than this difference, the predictions of the two models are similar at the late solidification stage.

Prediction of the CET in the Presence of the Melt Convection

In figure (4), the contour plot in the second column of the top row indicates the location where the first equiaxed grains nucleate in front of the columnar tips (white box). These grains locally block the advance of the columnar tips. As solidification proceeds, more and more equiaxed grains nucleate ahead of the columnar front, until at t = 4000 s (third column), equiaxed grains are present everywhere to the left of the red contour line that indicates the columnar front. These equiaxed grains block the columnar front along its entire length, and the red contour line therefore indicates the location of the CET in the casting.

The preeicted CET line is superimposed on the mid-thickness grain structure observed in the experiment in Figure (5). The white line in the figure indicates the boundary between the columnar

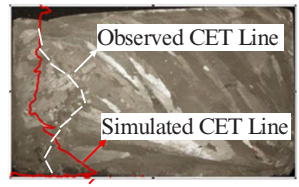

Figure 5. Simulated CET line (red) superimposed on the mid-thickness grain structure observed in the experiment [7]. The white line is an approximate indicator of the boundary observed between the columnar and the equiaxed grains in the grain structure.

and equiaxed grains observed in the experiment. It can be seen that the two lines are in reasonably good agreement. The reason for the slight disagreements at mid-height and at the bottom of the cavity are not entirely clear. The agreement can be expected to improve once the movement of equiaxed grains is accounted for in the model.

Conclusions

A three-phase Eulerian volume-averaged model for the CET in the presence of the melt convection is introduced. The model is validated by simulating the Sn - 3 wt. pct. Pb experiment of Hachani et al. [7]. The simulated cooling curves, including the recalescence at the location of one of the thermocouples, are in good agreement with the measurements. The results of the present model are compared with the results of a model where dendrite tip undercooling is neglected (Scheil model). The comparisons indicate that the role of tip undercooling is particularly noticeable at intermediate solidification stages. The position of the predicted CET contour is found to be in reasonably good agreement with the boundary between the equiaxed and columnar grains observed in the experiment. This agreement can be expected to improve once the movement of equiaxed grains is incorporated into the model.

References

1. J. A. Dantzig and M. Rappaz, *Solidification* (Lausanne, CRC Press, 2009), 430.

2. C.Y. Wang, and C. Beckermann, “Equiaxed Dendritic Solidification with Convection: Part I. Multiscale/Multiphase Modeling,” *Metallurgical and Materials Transactions A*, 27 (1996), 2754-2764.

3. C.Y. Wang, and C. Beckermann, “Prediction of Columnar to Equiaxed Transition during Diffusion-Controlled Dendritic Alloy Solidification,” *Metallurgical and Materials Transactions A*, 25 (1994), 1081-1093.

4. M.A. Martorano, C. Beckermann, and Ch.-A. Gandin, “A Solutal Interaction Mechanism for the Columnar-to-Equiaxed Transition in Alloy Solidification,” *Metallurgical and Materials Transactions A*, 34 (2003), 1657-1684.

5. M. Wu, A. Fjeld and A. Ludwig, “Modeling mixed columnar-equiaxed solidification with melt convection and grain sedimentation - Part I: Model description,” *Computational Materials Science*, 50 (2010), 32-42.

6. M. Wu, A. Fjeld and A. Ludwig, “Modeling mixed columnar-equiaxed solidification with melt convection and grain sedimentation - Part II: Illustrative modeling results and parameter studies,” *Computational Materials Science*, 50 (2010), 43-58.

7. L. Hachani, B. Saadi, X. Dong Wang, A. Nouri, K. Zaidat, A. Belgacem-Bouzida, L. Ayouni-Derouiche, G. Raimondi d, and Y. Fautrelle, “Experimental analysis of the solidification of Sn–3 wt. pct. Pb alloy under natural convection,” *International Journal of Heat and Mass Transfer*, 55 (2012), 1986-1996.

8. L. Hachani, K. Zaidat, B. Saadi, X.D. Wang, and Y. Fautrelle, “Solidification of Sn-Pb alloys: Experiments on the influence of the initial concentration,” *International Journal of Thermal Sciences*, 91 (2015), 34-38.

9. T. Carozzani, CH-A. Gandin, H. Digonnet, M. Bellet, K. Ziadat, and Y. Fautrelle, “Direct Simulation of a Solidification Benchmark Experiment,” *Metallurgical and Materials Transactions A*, 44(2013), 873-887.

10. D. Hoang, V. Steijn, L. Portela, M Kreutzer, C. Kleijn, “Benchmark numerical simulations of segmented two-phase flows in microchannels using the Volume of Fluid method,” *Computers & Fluids*, 86 (2013), 28–36.

11. J. Guo and C. Beckermann, “Three-dimensional simulation of freckle formation during binary alloy solidification: effect of mesh spacing,” *Numerical Heat Transfer, Part A*, 44 (2003), 559–576.